

Calibration of the Baikal Telescope NT200+ with the External Laser

Konstantin Antipin*

Moscow Engineering Physics Institute

konsty@gmail.com

September 17, 2006

Abstract

The NT200+ Telescope uses a single large-aperture laser, shooting into the water, to calibrate time-offsets of all NT+ photosensors to a precision of a few ns (distances from 70-180 m). We present an analysis of a first dedicated laser experiment, performed in spring 2006, to verify the method, check for possible systematic biases and give an in-situ determination of the laser emission limitations.

1 Introduction

1.1 Baikal Neutrino Telescope

The Baikal Neutrino Telescope is operated in Lake Baikal, Siberia, at a depth of 1.1 km. Deep Baikal water is characterized by an absorption length of $L_{abs}(480\text{nm}) = 20 \div 24$ m, a scattering length of $L_s = 30 \div 70$ m and a strongly anisotropic scattering function with a mean cosine of scat-

tering angle $0.85 \div 0.9$.

The first stage telescope configuration NT200 [1] was put into permanent operation on April 6th, 1998 and consists of 192 optical modules (OMs). An umbrella-like frame carries 8 strings, each with 24 pairwise arranged OMs, as shown in Figure 1 (central part). Four underwater electrical cables connect the detector with the shore station. Each optical module contains a 37-cm diameter QUASAR - photomultiplier (PM) which has been developed specially for this project [2]. The two PMs of a pair are switched in local coincidence in order to suppress background from bioluminescence and PM noise; each photomultiplier pair defines a channel.

With the NT200 telescope, a number of relevant physics results has been obtained so far [3]: searches for WIMPs, high energy atmospheric muon neutrinos and muons, relativistic and slow magnetic monopoles and diffuse extraterrestrial high energy neutrinos. The main physics result of NT200 is the all-flavor limit for a steady diffuse neutrino flux with E^{-2} shape [4].

*DESY-Summerstudent 2006; Supervisor: R. Wischnewski, Zh.A.M. Djilkibaev.

For NT200, the detection strategy for high energy neutrino events is based on a search for Cherenkov light from point-like cascades in a Mton-scale sensitive volume below the detector, which is much exceeding the instrumented geometric volume ($V_{geom}(NT200) \sim 0.1$ Mton).

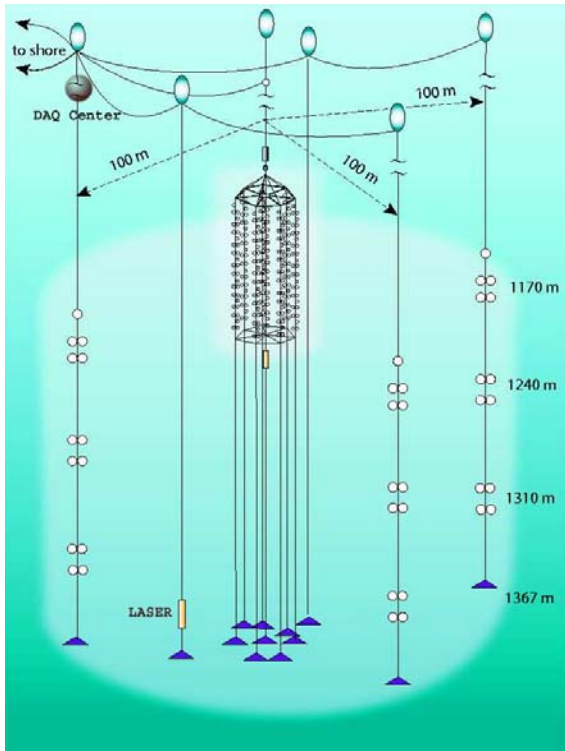


Figure 1: The upgraded Baikal Telescope NT200+ : The old NT200 surrounded by three external long strings at 100 m radius from the center. Also indicated is the external laser.

1.2 The NT200+ Telescope

The upgraded telescope NT200+ [5, 6] was put into operation in April, 2005. It consists of a central part (the old telescope

NT200) and three new, external strings (called “NT+”), as shown in Fig. 1. The external strings are 200 m long (140 m instrumented) and are placed at 100 m radial distance from the center of NT200. Each string contains 12 OMs, grouped in 6 channels (OM pairs) like in NT200. The upper channels are at approximately the same depth as the bottom ones of NT200. Adjacent channel distances are 20, 50, 20, 30 and 20 m from top to bottom along the string. All channels are down-looking, except the lower two on each string (up-looking). Numbering of channels in NT+ goes from top to bottom for each string (string 1: channel 1-6, string 2: channel 7-12, string 3: channel 13-18, respectively).

A trigger for NT200 is formed when the number of fired channels within 500 ns is at least 3. Each trigger pulse is sent from NT200 to NT+ (1.2 km cable), to allow offline sub-event synchronizations at ns-scale for both sub-detectors. On each external NT+ string, triggers are formed as independent string-triggers, in case of at least 2 channels fired within 1000 ns. The time jitter between channels from NT+ and NT200 is 2-3 ns, as verified by the external calibration laser.

1.3 Time calibration

Event reconstruction and classification are based on the precise light arrival times. Hence we need time calibration with precision of a few ns, in particular for the relative time-offsets between all channels. Time-offsets depend on PM-related settings (HV, thresholds), on cable lengths and delays of several electronic units. Calibration with ns accuracy and its independent verification

are obtained using a redundant calibration system. There are different tools for this purpose - external water laser, fiber laser in NT200, LED-Matrix units (with/without fibers).

Since the external laser is playing a large role, it is needed to verify that the standard calibration procedure introduces no systematic bias. For this purpose, a dedicated experiment was performed with the external laser and the NT+ strings in the context of the Baikal Ice-Expedition 2006.

This paper is devoted to the first analysis of these data. The main task is to proof, which channels (OMs) can be calibrated by the external laser in standard calibration runs. This means that in order to have precise time calibration for a given channel it is necessary to know that it really sees direct light from the laser. Scattered light would be the cause of systematic shifts in the time-offset determination. Thus, we should know for what laser emission angles α and laser intensity or distances a given channel does safely detect direct light. An in-situ measurement of the angular dependence of the laser intensity will also be useful. This work might yield recommendations for an improvement of calibration accuracy in standard laser runs by proper channel selection with α or amplitude criteria, or by cross checks. Also, suggestions for an optimized laser design, and/or an improved position of the laser relative to the strings can be helpful.

This work is organized as follows. In Sect. 2 we describe the existing laser, the dedicated laser experiment from April 2006 and the general procedure of laser event se-

lection. In Sect. 3 we present results of the amplitude analysis, including first results of the intensity angular dependence. Sect. 4 presents the time analysis, obtained treating the strings independently and for the whole detector. We discuss the evidence for direct light detection. Conclusions are drawn in Sect. 5.

2 Dedicated Laser Experiment in April 2006

2.1 NT200+ External Laser

For the NT200+ Telescope, the time-offset inter-string calibration (and for the outer strings also most of the intra-string calibration) is done with a powerful external laser light source with $> 10^{12}$ photons per pulse and ns-pulse duration, located between two outer strings and close to the lake bottom. See Fig. 1 for a sketch of the location, details are discussed below. Laser position and power ensure amplitudes of ~ 100 photoelectrons on at least a few PMTs on each external string and on NT200 simultaneously. High amplitudes minimize systematic calibration uncertainties due to light scattering.

The NT200+ laser calibration unit [7] is made of a powerful short-pulse Nitrogen laser ($\lambda = 337$ nm) with about $100 \mu J$ for < 1 ns pulse duration. It is pumping a Coumarin dye laser at 480 nm, which yields about 10% of the original intensity. After passing through a computer-controlled attenuator disk the light is isotropized by a light diffuser ball, made of a round-bottom flask filled with Silicone Gel (RTV-6156) admixed with hollow micro glass spheres at



Figure 2: The NT200+ external Laser before deployment in 2005. The white sphere inside the transparent pressure glass cylinder is the isotropizing ball.

about 5%-volume ratio. The total intensity loss of this isotropizing sphere is $\approx 25\%$. This guarantees that light output at maximum intensity is well above the design value of $> 10^{12}$ photons/pulse. An attenuator allows to operate the device with five gradually decreasing light pulse intensities

All components are mounted into a 1 m-long cylindrical glass pressure housing, which should give roughly isotropic emission for a large part of the upper hemisphere. Figure 2 gives a view of the assembled laser unit. The unit is installed on a separate string at a depth of 1290 m below surface (a depth just between outer string channels #4 and #5, see below). It is used for calibration throughout the year in

regular intervals, and is operating in an autonomous mode: after power-on from shore, a series of 200 pulses at 5 different intensities each, is conducted.

The construction of the external laser focused on maximal light output and a robust design, to guarantee long-term illumination on at least a few channels per string, rather than good uniformity of the light emission. Therefore, a mechanically and optically risky mounting of the isotropizing sphere outside the laser pressure glass housing was rejected. A pressure-stable new diffuser sphere is currently under longterm in-situ test at 1 km water depth.

The external laser was first installed together with commissioning of NT200+ in April 2005, and used, as described above, for time-offset calibration. It allowed also an independent performance check of the key elements of the NT200+ timing system. We measured the event-by-event relative time synchronization between all new strings and NT200, and found the jitter of this to be less than 3 ns. The laser can also be used to imitate light arrival time and amplitude patterns from high energy particle cascades (“point-like showers”) and to verify energy and vertex reconstruction. With the variation of the total intensity, a shower energy range from 20 TeV to 10 PeV can be covered.

2.2 The Experimental Setup

Figure 3 sketches the laser design with its elements relevant for this analysis: diffusive glass sphere (84 mm diameter), glass-cylinder (187 mm diameter), water-tightening black tape (which is non-transparent). As can be seen, some anisotropy for light

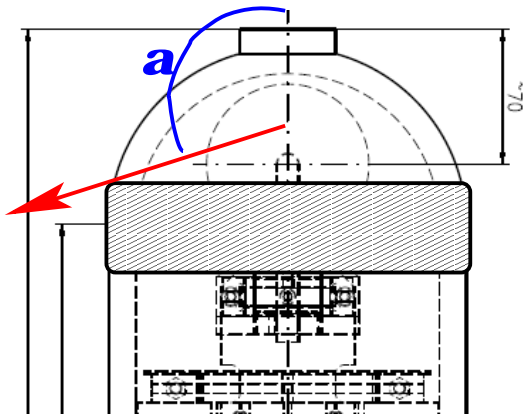


Figure 3: Sketch of the external laser design, see Fig.2. Indicated is α , the zenith angle for light emission towards a PM.

emission angles $\alpha > 90^\circ$ should be expected, up to the existence of “blind” (fully-screened) angular intervals. The situation is complicated, since for maximizing light output, light emission below the screening black tape is allowed by the design (i.e. partially compensating screening effects). Serious screening can lead to large contribution of scattered light for certain channels, which would yield systematic bias during the calibration of the relative time-offsets between channels. In the analysis of initial 2005 data (laser calibration and muon data), indications were found that some of the lower channels on the external strings (5th and 6th channels) might see non-direct light from the laser.

To check this assumption, a dedicated external laser experiment was made in April 2006. Four runs with four different laser z-position were carried out. Starting from the nominal laser position (“position 1”), the laser was moved upwards by 10m, 10m and 20m, respectively. Figure 4 gives the

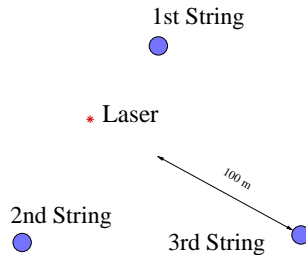


Figure 5: Top view of laser location and external strings for the NT200+ setup in 2006. NT200 is at the center (left arrow).

geometry of the setup, compare fig. 5 for a top view. Strings 2 and 3 are already in final position (deployment for 2006 was completed), string 1 is for technical reasons 20 m in vertical direction above it’s nominal position. As is evident from Fig. 4, the behavior of the channels at different laser emission angles α and distances R can be investigated; the following two figures elaborate this. Figure 6 gives the laser emission angle α for all channels and all laser positions. Obviously, α is increasing with the laser elevation. Since the first string is the closest to the laser, it covers the biggest range in α , for each individual channel as well as for the whole string. We can analyze laser emission characteristics in the range $25^\circ < \alpha < 135^\circ$. Figure 7 gives the distances to the laser, R, for all channels and all laser positions. Here, the behavior is less monotone than for α . Numbers below the first laser position indicate the channel number. The total range covered is R=65-180 m, the largest R difference seen by a single channel is ~ 35 m (1st string).

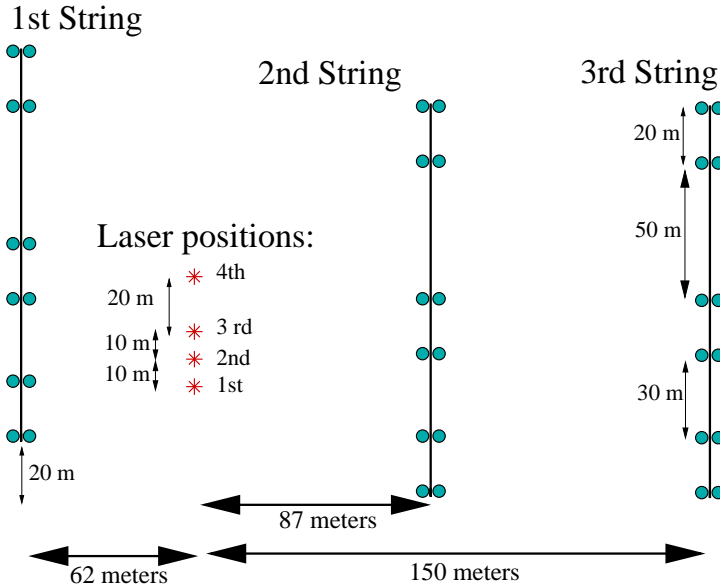


Figure 4: Relative positions of laser and external strings for the dedicated laser experiment (projected to laser-string plane).

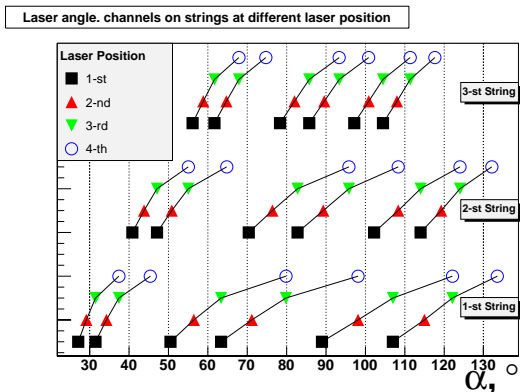


Figure 6: Laser emission angle α for all channels and laser positions (lines connect laser positions). For each string, channel numbering is from left to right (1-6,7-12,13-18).

The experiment was done on April, 8th, 2006 - during the last days of ice activity in Expedition 2006. In this period of deployment finalization, the telescope is not yet in its standard opera-

tion mode (which is reached after a 1-2 week setup/calibration procedure, that follows the Expedition closure every year). This implies that NT200+ is not operated at standard PM high voltages, nominal 0.3 photoelectrons (p.e.) thresholds; also no high precision calibration dataset is available, which would allow a determination of the true current settings (PM thresholds and precise absolute amplitude scale, in p.e.). As a good guess, and since many channels are close to their standard settings, the calibration constants obtained for the standard operation mode in 2006, are used for this analysis. Care has to be taken with direct amplitude interpretation, since deviations of the true absolute p.e.-scales can reach a factor of < 10 for worst channels. Precise time calibration data of the underwater TDCs (i.e. their count/ns-coefficients) are available, though. This

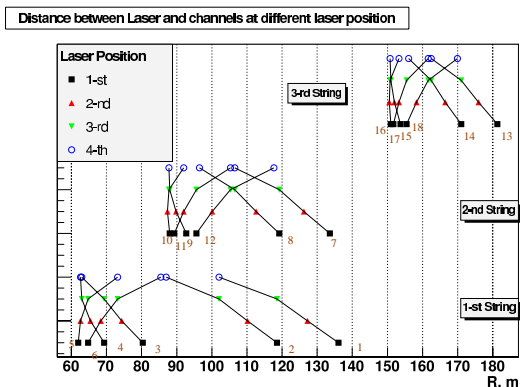


Figure 7: Distance R between laser and channels, for all laser positions (lines connect laser positions). Below each first laser position, the channel number is indicated.

means that time measurements will be possible with the standard ns-precision.

In this work, only data for NT+ (i.e. 3 external strings) are used, since NT200 was shut down at the time of these runs. Five channels (channels 4,6,9,17,18) are operated with one PM per channel only (the standard mode for channels with one malfunctioning PM). This implies they are set to a higher threshold (few p.e.), to operate at acceptable dark noise rates.

2.3 Data analysis

Experimental data from the 4 runs (h4093-h4096) for the laser positions 1-4, respectively, have been processed through the standard Baikal data-analysis chain, and converted to paw-ntuples afterwards. The analysis presented here was performed using the ROOT package [8], with scripts written by the author.

In step 1 of the analysis the events origi-

nating from the laser are separated from the atmospheric muon background events, and the 5 laser intensities are split. Laser event tagging is easily done by a single cut in N_{hit} , the number channels that were hit for a given event. Figure 8 demonstrates (for the first laser position, run h4093), how clearly muon background events are rejected with a cut $N_{hit} > 9$. Separation of events from

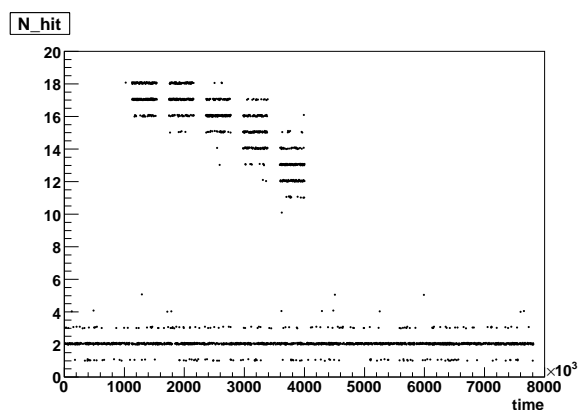


Figure 8: Number of hit channels, N_{hit} , vs. run time for the first run (time in 0.1ms, ~ 13 min in total). Laser Intensities $I_1 > I_2 > \dots > I_5$ lead to decreasing N_{hit} vs. time.

different laser intensities was made by time tagging: the laser has a fixed interval between series and also a fixed series duration. For the second run (h4094) some instabilities during data taking were observed (due to a DAQ malfunctioning, and not related to the laser), which led to a loss of the 3rd and most of the 2nd laser intensity for this laser position. For this run, amplitudes on selected channels were used for laser intensity separation (I_1, I_4, I_5).

The combined trigger and selection efficiency of laser events is very high: for three runs (excluding the 2nd run), 2998 laser

events are found - compared to 3000 expected (3 runs \times 5 intensities \times 200 events). This corresponds to an efficiency of 99,9%.

3 Amplitude analysis

3.1 Channel selection

The amplitude analysis was preceded by selecting channels with reliable amplitude information, checking all laser intensities and all laser positions.

3.1.1 Overflow and very small amplitudes

Each channel has its own amplitude threshold and dynamic range. First of all, we check if the measured amplitudes are within the dynamic range of the channel. Figure 9

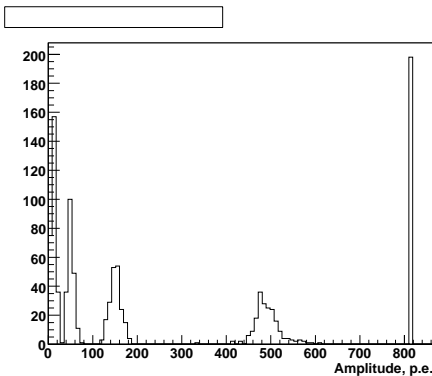


Figure 9: Amplitude distribution for channel #1 in 1st laser position.

illustrates a typical amplitude distribution for one channel, which shows all five different laser intensities. Amplitudes related to the first (most powerful) laser intensity exceed the dynamic range of that channel and are therefore excluded from analysis. Also those amplitude distributions

which are (partly) suppressed by the amplitude threshold of channels are excluded from analysis.

3.1.2 Linearity of amplitude response

The amplitude analysis, which should verify the isotropic behavior of laser intensity, requires reliable linearity of amplitude measuring system of each channel. Amplitude linearities of channels were checked in the following way.

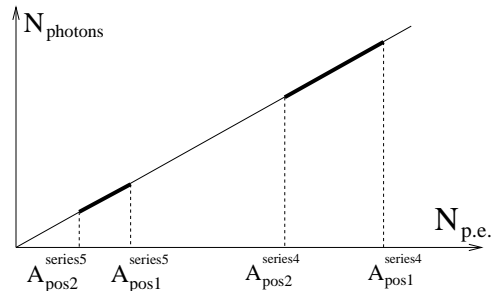


Figure 10: Conversion from number of photons to amplitudes in photoelectrons, for the case of linearity.

Taken the amplitudes measured by a given channel for two laser positions i and j and laser intensity n , the ratio $\delta_{ij}^n = A_i^n / A_j^n$ has been calculated. This ratio has to be the same for different laser intensities, if the amplitude response is linear. This statement is illustrated on Figure 10. As a measure of nonlinearity of channels we use the asymmetry η , defined as

$$\eta = (\delta_{ij}^n - \delta_{ij}^k) / (\delta_{ij}^n + \delta_{ij}^k),$$

where n and k indicate different laser intensities.

In Figure 11 one can see the values of η , calculated for different amplitude ranges for

channel #1. Amplitudes, that were taken for calculating η are indicated by markers. For the majority of channels, absolute values of η are less then 0.02. But for some channels we get much bigger values. Channel #11 is one of these channels, see Fig. 12. As it is shown in Figure 12, the value of asymmetry rises significantly when the smallest measured amplitude is used in η calculation. From this estimation of channel nonlinearity, channel #7 was excluded from analysis, as well as the smallest amplitudes in channels #11, #16 and #17.

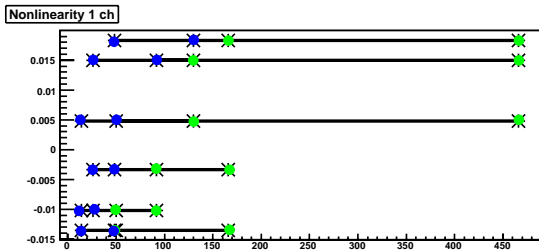


Figure 11: Asymmetry η for channel #1 - example of linearity for full amplitude range.

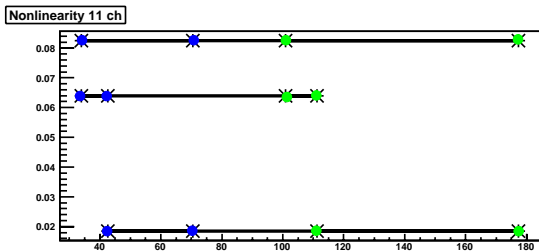


Figure 12: Asymmetry η for channel #11 - example of non-linearity for Small amplitudes.

3.1.3 Laser position 4 for 2nd string

During the analysis described in the Sect. 3.1.2., a strange behavior of the amplitudes on 2nd string was discovered. For the geometry of this experiment (Figure 13), we expect that amplitudes on channels #7 and #8 should increase and on the channels #11 and #12 decrease, when changing the laser position from position 1 to 4. But the experimental values behave differ-

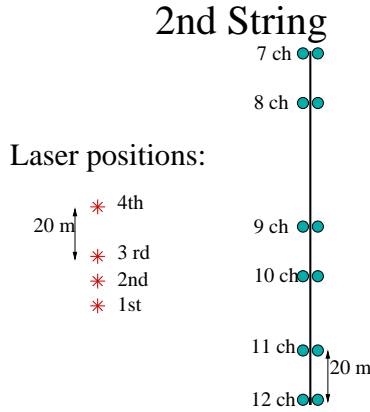


Figure 13: 2nd String and laser positions.

ent. As can be seen from Table 1, for the 4th laser position amplitudes on all channels do abruptly decrease, compared to 3rd laser position. Laser intensities shown in Table 1 are: for channel #7 - 5th intensity, channel #8 - 5th, channel #10 - 5th, channel #11 - 4th, and for channel #12 - 4th intensity.

This fact is unusual, especially for the upper channels - since the laser is coming closer, there is no obvious reasons for decreasing amplitudes. A sudden laser performance degradation is excluded, since this phenomenon is observed only for the 2nd string. Another possible explanation is that the laser at the 4th position is screened for the 2nd string by some external laser con-

Table 1: Amplitudes for 2nd string and laser positions 1-4.

Position	Channel				
	7	8	10	11	12
1	60	59	159	177	163
2	67	69	142	111	117
3	86	205	119	101	95
4	64	132	17	16	8

struction elements (no obvious candidates exists, though), or that the diffuser ball has a local “blind spot” on it’s surface. In case of screening, this should be reflected in the light arrival times measured for the 2nd string.

3.2 Analysis of non-isotropy of the laser

For a point-like isotropic source of light (laser source in our case), the amplitude in photoelectrons (p.e.), $A_{p.e.}$, measured by an optical module (OM), which is located at distance R from the source, is given by

$$A_{p.e.} = I * exp(-R/L) * f(\cos \theta) / R^2 * const \quad (1)$$

where L is the absorption length, I - the light source intensity, and $f(\cos \theta)$ - the angular sensitivity of the OM (θ is the light incidence angle on the OM, as given in Fig. 14). Expression (1) may be rewritten as follows:

$$F(R) = \ln(A * R^2 / f(\cos \theta)) = -R/L + Const \quad (2)$$

The function $F(R)$ depends linearly on R , with a slope defined by the absorption length L for an isotropic source. If the light source intensity $I(\alpha)$ depends on the emission angle α , the linearity of $F(R)$ would

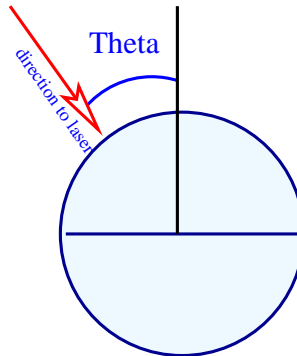


Figure 14: Light incidence angle θ on the Optical Module (OM).

be broken. Our analysis strategy of non-isotropic behavior of laser source intensity is the following.

During the first step, the function $F(R)$ is calculated for each channel for the four different laser locations. Results for channels located on the third string are shown on Figure 15. As shown, $F(R)$ has a different behavior and/or offset (normalization) for different channels.

In a second step we normalize $F(R)$ of nearby channels to each other. For illustration of this procedure let us consider neighboring channels on the second string (channels #11 and #12, see Fig. 13). Relative location of laser in 1st position and channel 12 is symmetrical to the location of laser in position 3 and channel 11. This allows, to normalize $F(R)$ distributions of these channels as shown in Figure 15 (arrows illustrate the normalization of two symmetrical locations). Applying this procedure to all nearby channels, a combined distribution of $F(R)$ for the whole string has been obtained. The distribution for the third string is shown on Figure 16. It significantly dif-

fers from the linear one, expected for an isotropic source. This indicates an angular dependence of the laser source intensity.

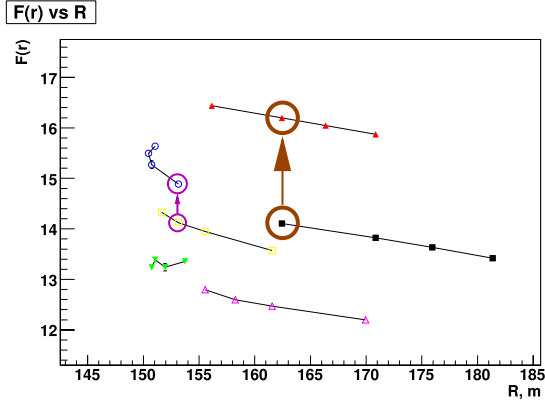


Figure 15: $F(R) = \ln(A * R^2 / f(\cos\theta))$ for 3rd string and all laser positions. The suggested normalization procedure for nearby channels is indicated.

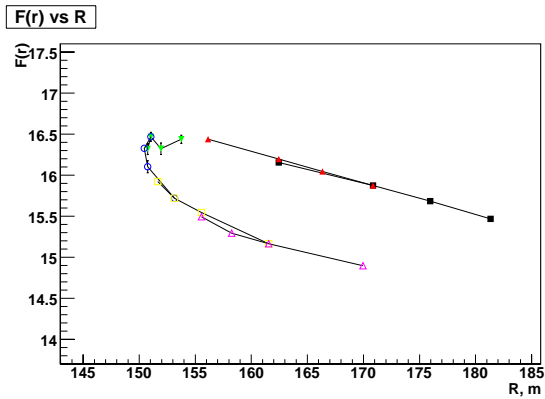


Figure 16: $F(R) = \ln(A * R^2 / f(\cos\theta))$ for 3rd string and all laser positions, after relative normalization (see text).

Using the amplitude $A_{p.e.}$ measured for a given channel and applying the above described approximate normalization procedure, the laser intensity as function of emis-

sion angle α , $I(\alpha)$, can be calculated from (1). For this analysis, an absorption length of $L = 18$ m was used, as derived from the slope of function $F(R)$ for the 1st channel on the 1st string. For this channel the angular range is $\alpha = 27 - 38^\circ$ (the smallest values among all channels), and the angular behavior of the laser source intensity is close to an isotropic one.

The obtained angular distribution of laser source intensity $I(\alpha)$ is shown in Figure 17. The black, red and green markers on this picture correspond to channels on first, second and third strings, respectively. Points corresponding to different strings are normalized one to another assuming smoothness of the distribution. As one can see from Fig.17, the laser source intensity is quasi isotropic for $\alpha < 50^\circ$. For $\alpha > 50^\circ$, the intensity significantly decreases with α . We note, that the quantitative results obtained here might depend on details of the particular intra- and inter-string amplitude normalization procedure chosen.

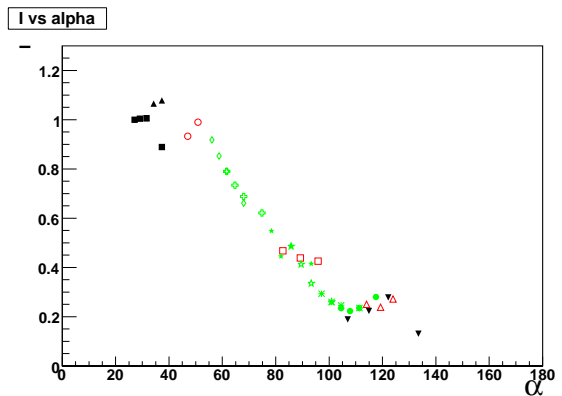


Figure 17: Angular dependence of laser source intensity $I(\alpha)$.

4 Time response analysis

4.1 Reference channel

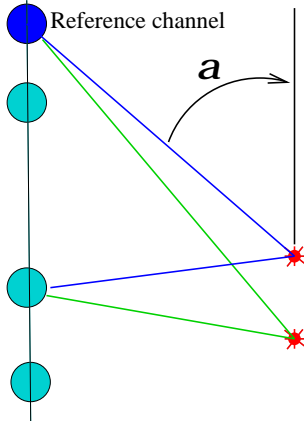


Figure 18: Time differences δt_{ki} with respect to one reference channel per string.

The amplitude analysis indicates a non-isotropic behavior of the laser source intensity for angles $\alpha > 50^\circ$, which may be due to an intrinsic non-isotropy of the light diffuser ball, or caused by partial screening of the light emitting ball by construction elements of the laser (see Fig. 3). The main goal of the time analysis is (1) to verify the validity of the standard time-offset calibration procedure (assumption of direct light detection) for all channels, and (2) to estimate the influence of such possible screening on the arrival time distribution of detected photons.

Since the time of the laser pulse is not known, we analyze the difference of light arrival times on pairs of channels: $\delta t_{ki} = t_k - t_i$. To exclude the relative time-offset between different strings, we use one reference channel per string (see Figure 18): on 1st string - channel #1, on 2nd string

- channel #8 and on 3rd string - channel #13. Thus we have 15 time distributions for each laser position. To investigate scattering in Sect. 4.2, we use a reference channel on string 1.

4.2 Light scattering in water

As it was mentioned earlier, deep Baikal water is characterized by an absorption length of 20 - 24 m, a large scattering length $\sim 30 - 70$ m and a strongly anisotropic scattering function. In general, scattering leads to a delay of photon arrival times and increases the dispersion of the arrival time distribution. In case of deep Baikal water, scattering is small and becomes important only at a large distances from the light source. Mean value and dispersion of

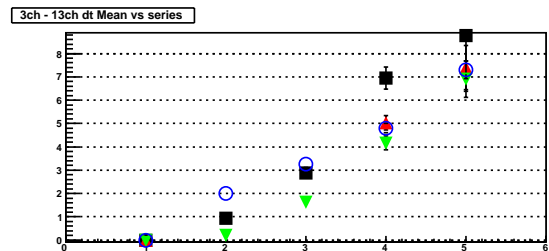


Figure 19: Difference of mean arrival times, $\langle \delta_{13-3} \rangle$, on channel 13 (180 m from laser) and channel 3 as function of laser intensity number ($I_1 > I_2 > I_3 > I_4 > I_5$).

the time distribution of detected photons depend on the intensity of light flux (i.e. on the amplitude measured by the optical module). Thus, at low amplitudes, mean value and dispersion of the arrival time distribution for large distances could be significantly larger than for direct (non scattered) photons. Shown in Figure 19 are the differences $\langle \delta_{13-3} \rangle = \langle t_{13} - t_3 \rangle$ of mean

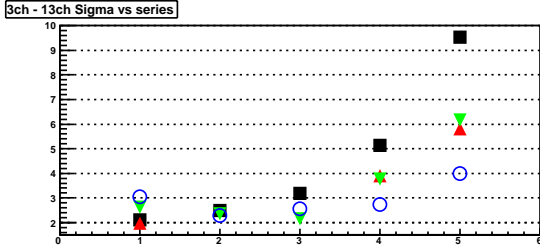


Figure 20: $\sigma_{\delta_{13-3}}$ as function of laser intensity.

arrival times measured by channel #13 (located 180 m away from the laser) and for reference channel #3 (located close to the laser), for different laser intensities and different laser positions. To compare the relative behavior of $\langle \delta_{13-3} \rangle$ for fixed positions, the first intensity data point for each laser position was normalized to 0. The black, red, green and blue markers correspond to 1st, 2nd, 3rd and 4th laser positions, respectively. Dispersions of the time difference distributions are shown in Fig. 20. In case of channel #13 we don't expect any screening effects, and interpret the increase of $\langle \delta_{13-3} \rangle$ and $\sigma_{\delta_{13-3}}$ with decreasing intensity as the result of light scattering in water over big distances.

4.3 Expected times

If we imagine the laser source as an isotropic high intensity source of light without any kind of screening (i.e. all channels see direct light), then we can calculate expected light arrival time differences for selected pairs of channels by $\delta t_{expect} = \Delta R / v_{water}$, where ΔR - difference of distances from laser to the two channels, and $v_{water} = 0.2188$ m/ns - speed of light in deep water of Lake Baikal. Figure 21 shows expected and experimen-

tal time differences depending on the laser position for channel #18 (first experimental data point is normalized to the expected one).

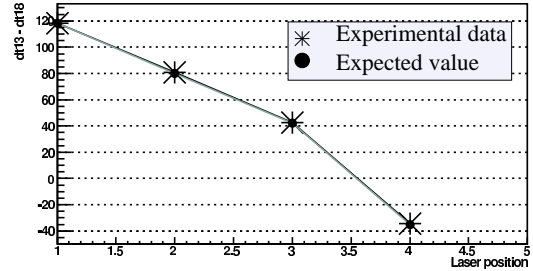


Figure 21: Expected and experimental time differences vs laser position for channel #13 (reference channel #18).

From similar distributions for all channels we conclude, that the deviation from expected values is mostly less than a few ns. For a more precise analysis we plot the deviation itself: $\tau = \delta t_{expect} - \delta t_{exper}$. In order to analyze the laser source isotropy, we need to look at τ against zenith angle α . Figure 22 presents τ , the difference of measured arrival times w.r.t. the expected, for all channels at all different laser positions, and all laser intensities (always regarding the reference channel on that string). As in Fig. 21, data points for every first laser position are normalized to 0. Numbers on the figure indicate corresponding channels numbers, different colors of the markers relate to different laser positions. As an example, let's take 1st series on the first string (top left panel). The first point on this plot (black marker) corresponds to channel #2 for 1st laser position, second point (red) - corresponds to channel #2 for 2nd laser position. The fourth point (black) corre-

sponds to channel #3 for 1st laser position, and so on. Red points (2nd laser position) are missing in the plot for second and third laser intensities (see Sect. 2.3).

For the first string, the time deviation τ is not more than 2 ns (except one point).

Considering lowest channels on second string (channels #11 and #12), one can see from Figure 22 that the time deviation τ increases with decreasing intensity for 4th laser position and the three lowest laser intensities. This fact could be explained by light scattering in water. But we should understand, if this is only an effect of light scattering, or if there is another contribution which is caused by some kind of screening. We remind, that for the 4th laser position, amplitudes measured by all channels on the second string are abnormally low, see Sect. 3.1.3. We have to analyze the time delay versus measured amplitudes. For that purpose we use the following strategy.

Since amplitudes are small, channels #11 and #12 detect only about 20% - 80% of all laser events. This implies that mean amplitudes are close to the threshold of the channel (~ 1 p.e.). Assuming that amplitudes follow a Poisson distribution, we can estimate the mean value of the amplitude $\langle A \rangle$. Since the channel detects only n events (from a total number of $N = 200$), we can calculate the probability that channel doesn't detect the laser pulse as $P = 1 - n/N$. Also for Poisson distribution one can determine the same probability as $P = e^{-\langle A \rangle}$. Thus we obtain an estimate for $\langle A \rangle = \ln(\frac{N-n}{N})$. Now let us consider the time difference defined as $dt = t_{ch-ref, \mathcal{L}h}^i - t_{ch-ref, \mathcal{L}h}^1$, where superscripts indicate the laser intensity. As it was discussed earlier, for channel #13 the

time delays are caused by light scattering. Due to big distance from laser, the time delay for this channel rises up to ~ 10 ns for lowest laser intensity. In contrast, channels #11 and #12 are located closer to the laser source. Thus, the contribution of scattering to time delays is less than for channel #13. But as it is shown in Figure 23, for these channels we see significantly bigger time delays for all amplitudes. This indicates, that probably some kind of screening affects the time distributions of channels #11 and #12 on the second string for the 4th laser position and low laser intensities.

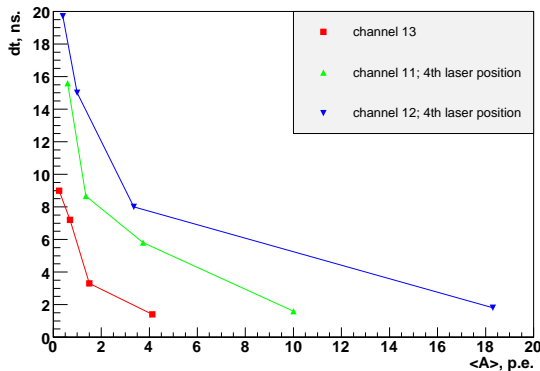


Figure 23: Time delay vs amplitude for channel #13 (water scattering) and for channels #11 and #12.

On the third string, for lower channels, we also see time deviations from expected values (Figure 22), but the values of this deviations are consistent with expectations from light scattering in water.

The results of the time analysis show, that light scattering in water, as well as some possible screening effects in the laser source do not influence the time distributions of photons for higher laser intensities. This allows to use the external laser for

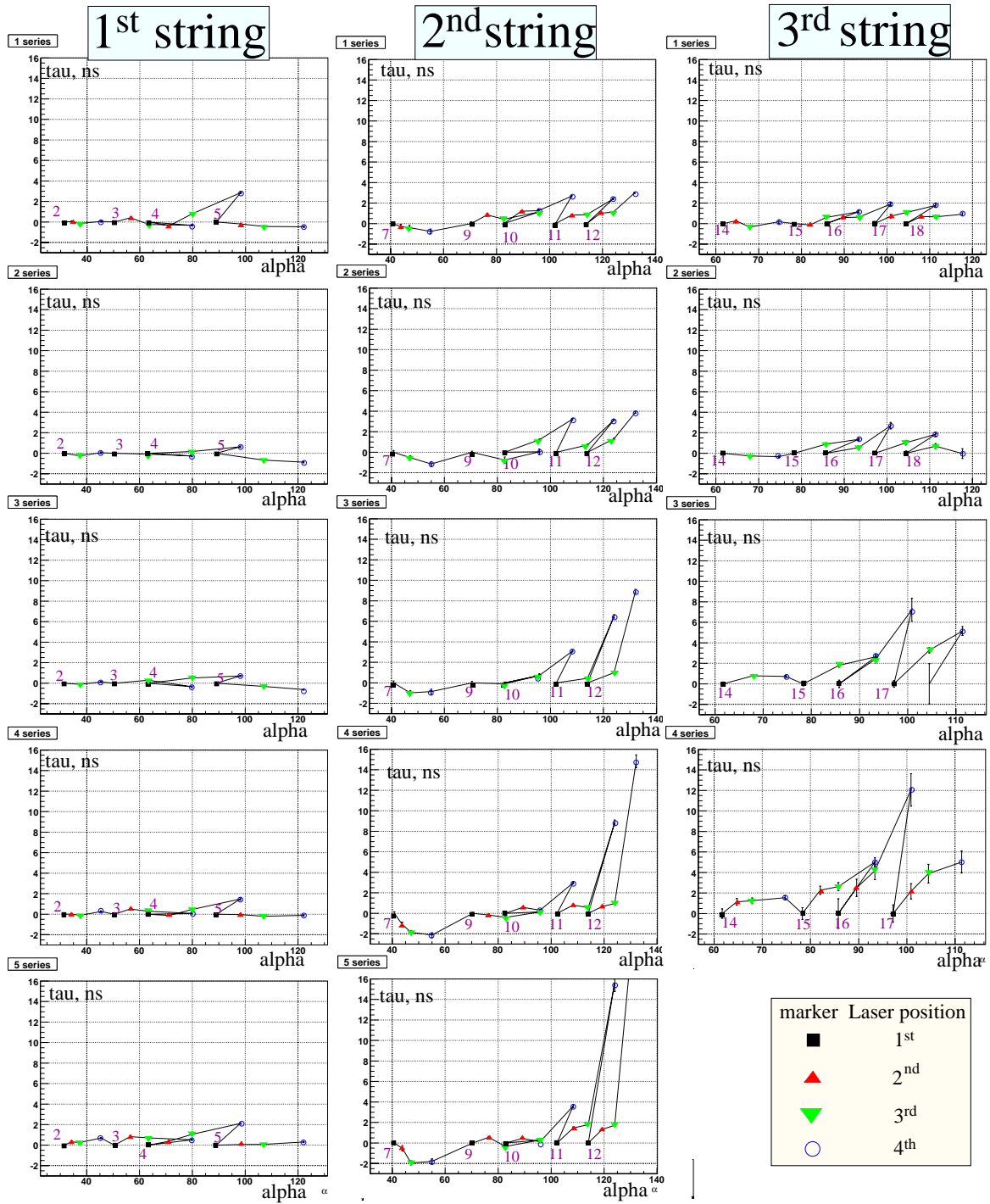


Figure 22: Difference of measured and expected arrival times, τ , as function of laser emission angle α , for all channels, all different laser positions and laser intensities.

time calibration of the neutrino telescope NT200+. The unexpected time deviations which have been observed for the 4th laser position and the lowest laser intensities may be explained by some kind of “screening” of the laser source. However, this preliminary conclusion requires an additional analysis.

5 Conclusion

During the Baikal Winter Expedition in April, 2006, a dedicated experiment with the external laser and the NT+ strings was performed. The main goal of this experiment was (1) a verification of the standard time-offset calibration procedure, that uses the external laser and assumes direct light detection, and (2) an investigation of the angular distribution of photons emitted by the laser light source. The following preliminary results are obtained.

An analysis of the amplitude information, based on an approximate inter-calibration procedure, was performed and results in a measurement of the angular dependence of the laser intensity. The intensity of the laser light source is quasi isotropic for zenith angles $\alpha < 50^\circ$. For $\alpha > 50^\circ$, light intensity decreases continuously with α . The intensity at $\alpha \approx 120^\circ$ is about 5 times lower than at $\alpha = 30^\circ$. Some of these conclusions can be verified, once fully calibrated standard laser data from 2006 are available.

The analysis of data based on the time information shows that the angular-dependent light intensity and scattering processes in water do not influence significantly the arrival times of photons for highest laser intensities. This allows to use the external laser in its standard position and

with the standard procedure, to obtain the time-offset calibration of the whole neutrino telescope NT200+.

Acknowledgment

Allow me to thank my supervisor Dr. Ralf Wischnewski for continuous support and encouragement during this project. Without his help and guidance it is hard to imagine this project to come to its final conclusion.

I also truly enjoyed working with Prof. Zhan Magisovich Dzhilkibaev - his in-depth comments helped me to learn a lot during this summer. Thanks to all summer students - time, that I spend here, is unforgettable. Also I am grateful to Mr. Hiller and Mrs. Baer for their organization work. I had a great experience during the program.

References

- [1] Belolaptikov I *et al.* 1997 *Astropart. Phys.* **7** 263
- [2] Bagdjev R *et al.* 1999 *Nucl. Instrum. Methods* **A420** 138.
- [3] Aynutdinov V *et al.* *Proc. of IInd VLVNT Workshop*, November 2005 Catania Italy; *Nucl. Instrum. Methods* (2006), in press.
- [4] Aynutdinov V *et al.* 2006 *Astropart. Phys.* **25** 140
- [5] Aynutdinov V *et al.* 2005 *Proc. of V Int. Conf. on Non-Accelerator New Physics* June 7-10 Dubna Russia

- [6] Aynutdinov V *et al.* *Proc. of Ind VLVNT Workshop*, November 2005 Catania Italy; *Nucl. Instrum. Methods* (2006), in press.
- [7] Aynutdinov V *et al.* *Proc. XXth ICRC, vol.5, p.231* August 2005 Pune India, astro-ph/0507115
- [8] <http://root.cern.ch/root/>